Spin polarization and magnetic dichroism in photoemission from core and valence states in localized magnetic systems. II. Emission from open shells

Gerrit van der Laan

Daresbury Laboratory, Warrington WA4 4AD, United Kingdom

B. T. Thole

Materials Science Center, University of Groningen, 9747 AG Groningen, The Netherlands
(Received 15 December 1992)

With the use of many-particle theory general equations are derived for the six fundamental spectra, which are special linear combinations of the spin-polarized photoemission spectra measured with left-, Z-, and right-circularly polarized radiation. These fundamental spectra, which are the isotropic spectrum, spin spectrum, magnetic circular dichroism, spin-orbit spectrum, anisotropic spectrum, and anisotropic spin spectrum give the correlation between the spin, orbital, and quadrupole momenta in the ground state and spin and orbit of the hole created after photoemission. For emission from an incompletely filled shell the integrated intensities of the fundamental spectra are proportional to the expectation values of the number of electrons, spin magnetic moment, orbital magnetic moment, the alignment between orbital and spin magnetic moment, the quadrupole moment, and the correlation between quadrupole and spin magnetic moment, respectively. This can be used to study the magnetic anisotropy of localized magnetic systems. We calculated the fundamental spectra for the $4f$ photoemission of the rare-earth ions and show that the multiplet structure displays a strong polarization dependence in agreement with our analysis in terms of correlations of moments and the rules for the integrated intensities. Finally we present the relation between the polarization effects in inverse photoemission and normal photoemission and we discuss the magnetic dichroism in metallic iron, cobalt, and nickel.

I. INTRODUCTION

The understanding of the magnetic anisotropy in magnetic bulk materials, multilayers, thin films, and surfaces is of great technological importance.[1] An example is the application of magnetic films for magnetic and magneto-optical recording with in-plane and perpendicular magnetization direction, respectively. These materials display a large magnetostriction, which is connected to the orbital magnetic moment of the unpaired electrons. Consequently, there has been a major interest in the separation of the orbital and spin contributions to the magnetic moment. Using neutron scattering the spin and orbital contributions can be separated by fitting the measured form factors to a suitable model.[2,3] Using x-ray scattering in an antiferromagnet the magnetic superlattice reflections can be decoupled from the structural Bragg peaks.[4,5] In ferro- and ferrimagnets the charge and magnetic Bragg peaks coincide, so that the latter are swamped, but a first-order interference term exists if the structure factor is complex, or if the radiation source is circularly polarized. The key to the separation of the spin and orbital magnetization lies here in the different dependence on the Bragg angle, which can be tuned by the photon energy.[6,7] However, attempts to implement a quantitative analysis experimentally have been, so far, inconclusive.[8,9]

Recently, it has been shown that the spin and orbital magnetic momenta can be separated using circular magnetic x-ray dichroism (CMXD). Thole *et al.*[10] derived a sum rule which states that the integrated circular dichroism signal is proportional to the orbital magnetic moment per hole. This sum rule has been demonstrated on ferromagnetic nickel.[11] The Ni $2p$ CMXD spectrum consists of two structures corresponding to excitations from the $2p_{3/2}$ and $2p_{1/2}$ levels into the unoccupied $3d$ states above the Fermi level which are mainly of minority spin character. Without $3d$ spin-orbit interaction the $2p_{3/2}$ and $2p_{1/2}$ peaks have equal intensities with opposite signs, thus the integrated signal is equal to zero. In the presence of the $3d$ spin-orbit interaction, the valence holes have predominantly $3d_{5/2}$ character and the $2p_{3/2}$ peak increases and the $2p_{1/2}$ peak decreases in absolute intensity resulting in an integrated intensity which can be related to an orbital moment of $0.053\mu_B$,[12,13] in good agreement with neutron-diffraction[14] and local spin-density calculations.[15] There are also sum rules which relate the branching ratio of the isotropic spectrum and the circular dichroism to the ground-state expectation values of the spin-orbit interaction[16] and the spin magnetic moment,[17] respectively. Depending on the character of the state to which the core electron is excited, the spectral shape of the magnetic x-ray dichroism can be calculated either by a one-particle or by a many-electron approach. Local-density-functional theory, such as a relativistic Korringa-Kohn-Rostoker Green's-function method[18-21] as well as multiple-scattering theory,[22,23] give a good agreement for rare-earth L edges and transition-metal K edges. However, a many-electron approach is required to

explain the multiplet and satellite structures, which are observed in the rare-earth M edges and the $3d$ transition-metal L edges.[12,13,24−39]

After the experimental proof of magnetic x-ray dichroism in 1986,[25] a surge of interest in related phenomena in the x-ray region arose, such as resonant magnetic x-ray scattering,[40] magnetic Kerr effect,[41] and Faraday rotation.[42] In 1990 Baumgarten et al. observed circular dichroism in x-ray photoemission (CDXPS) in the Fe $2p$ level of ferromagnetic iron.[43] In photoemission the excited electron has no interaction with the remaining system and the dichroism requires, apart from core or valence spin-orbit interaction, an electrostatic interaction between the core level and the polarized valence levels.[44,45] This is a fundamental difference with CMXD where not only electrostatic interaction gives dichroism, but large effects occur also because the excited electron is subjected to the Pauli exclusion principle. The different electrons produced by the left- and right-circularly polarized light have different probabilities for excitation into the valence shell.

In a previous paper[46] (referred to as paper I), we presented a general analysis of magnetic dichroism and spin polarization in core level and valence-band photoemission. It was shown that circular dichroism in core-level photoemission requires a correlation between the spin S_v of the valence band, on which the magnetic field acts, and the orbital momentum L_c of the core hole, on which the photon polarization acts. For deep core levels the core-valence exchange interaction couples S_v with the core-hole spin S_c and the core-hole spin-orbit interaction couples S_c with L_c. The spin-orbit interaction aligns S_c and L_c parallel in the $j = l + \frac{1}{2}$ and antiparallel in the $j = l - \frac{1}{2}$ core level. Except for the sign change between these two edges, the CDXPS spectrum will be similar to the spin-polarized core-level photoemission, which gives the correlation between S_v and S_c.[44−48] The circular dichroism of a deep core level can also be obtained by a one-electron model.[49] However, for a shallow core level, where the core spin-orbit interaction is small compared to the core-valence Coulomb and exchange interactions, a many-electron approach is essential using Coulomb interactions to couple L_c to L_v and the valence spin-orbit interaction to couple the latter to S_v. The CDXPS spectrum is then strongly dependent on the valence-band spin-orbit coupling to produce the orbital magnetic moment.[50]

In this paper we will treat the emission from an open shell, specializing to the $4f$ shell in the rare earths. In an open shell the electrons are subjected to the Pauli exclusion principle and have mutual Coulomb repulsion. We can consider the photoemission from the open shell as the particle-hole partner of x-ray absorption where the core shell is replaced by a continuum shell. Therefore, photoemission with polarized radiation offers advantages similar to x-ray absorption, such as the possibility to determine the expectation value of the orbital and quadrupole momenta in the ground state.[10] Contrary to the core level, the continuum state has no spin-orbit interaction. However, the spin magnetic moment which in

CMXD is obtained from the spin-orbit split core-level branching ratio,[17] can in photoemission be obtained by resolving the spin of the photoelectron.

This paper is organized as follows. In Sec. II, we derive general results for spin-photon polarized photoemission spectra. We give equations for the integrated intensities of the fundamental spectra as well as for the individual peak intensities in LS coupling. We discuss the consequences of the symmetry breaking by, e.g., spin-orbit and crystal-field interaction and treat the dependence on the emission angle. To illustrate the theory we give in Sec. III the calculated spin-photon polarized $4f$ photoemission of the rare earths, which are an ideal example because the $4f$ wave function is strongly localized and its photoemission displays a clear multiplet structure due to the strong Coulomb interactions between the $4f$ electrons. The spectral trends in the fundamental spectra are discussed and the integrated intensities are related to the expectation values of the spin, orbital, and quadrupole moment. In Sec. IV, we treat the spin-photon polarization of inverse photoemission, and in Sec. V we give some prospects for the study of $3d$ and $5f$ materials. Conclusions are given in Sec. VI.

II. THEORY

We will derive the expressions for the polarized photoemission under very general assumptions. The main restrictions are that we take into account only one final-state channel ($\Delta l = +1$ or -1), and a constant radial matrix element for electron excitation to the continuum. For photoemission far above the continuum onset the $\Delta l = +1$ channel dominates and there are only minor variations of the radial matrix elements with energy, thus the error in these approximations is small. Further we assume that the emission from one valence shell can be separated from other emissions in the spectrum.

Consider any state $\langle \psi |$ containing electrons in a shell with angular momentum l, such as a partly filled l band or a mixture of l^n, $l^{n+1}\underline{v}$, $l^{n+2}\underline{v}^2$, where $\underline{v}$ denotes a hole in any shell that has no dipole matrix element with the continuum shell $c = l \pm 1$. $\langle \psi |$ may have any other open spectator shell, but has no continuum electrons in c. The dipole matrix element for transition from a ground state $\langle \psi |$ to a final state $| \psi' c m' \sigma' \rangle$ is

$$D_{m'q\sigma'} = \sum_{m\sigma} \langle \psi | l^{\dagger}_{m\sigma} c_{m'\sigma'} | \psi' c m \sigma' \rangle \langle lm\sigma | rC^{(1)}_q | cm'\sigma' \rangle$$

$$= \sum_{m\sigma} \langle \psi | l^{\dagger}_{m\sigma} | \psi' \rangle \langle lm\sigma | rC^{(1)}_q | cm'\sigma' \rangle , \qquad (1)$$

where $C^{(1)}_q$ is a normalized spherical harmonic, and $q = -1$, 0, $+1$ denotes right-circularly, Z-, and left-circularly polarized radiation, respectively. The $l^{\dagger}_{m\sigma}$ and $c_{m\sigma}$ denote the creation and annihilation operator for an l

shell and c continuum electron, respectively. The quantization axis to which q and the orbital components m and m' refer is the z axis, whereas the spin components σ and σ' refer to the axis z' with respect to which the spin polarization is measured and which need not be equal to z.

A. Integrated photoemission spectra

The integrated intensity ρ for a fixed value of σ' can be derived by summing the square of Eq. (1) over all ψ' and m':

$$\rho_{q\sigma'} = \sum_{\psi'm'} |D_{m'q\sigma'}|^2 = \sum_{\psi'm'} \sum_{m\sigma m\sigma} \langle\psi|l^\dagger_{m\sigma}|\psi'\rangle\langle\psi'|l_{\underline{m}\underline{\sigma}}|\psi\rangle\langle lm\sigma|rC^{(1)}_q|cm'\sigma'\rangle\langle cm'\sigma'|rC^{(1)}_{-q}|l\underline{m}\,\underline{\sigma}\rangle$$

$$= \sum_{m\sigma}\langle\psi|l^\dagger_{m\sigma}l_{m\sigma}|\psi\rangle\sum_{m'}|\langle lm\sigma|rC^{(1)}_q|cm'\sigma'\rangle|^2 = \sum_{m\sigma}\langle n_{m\sigma}\rangle\rho_{m\sigma q\sigma'} \, , \tag{2}$$

where in the last step we extended the summation over ψ' to all states, including those with c electrons, because these states give no matrix elements.[51] Therefore, this summation can be removed using the closure relation. Thus, the integrated intensity $\rho_{q\sigma'}$ is the sum over each $m\sigma$ sublevel of its occupation number n times the total transition probability ρ from that sublevel to the c shell. Apart from the radial integral, the intensities $lm\sigma \rightarrow cm'\sigma'$ are given by the Wigner-Eckart theorem as a squared 3-j symbol times a Kronecker delta for the spin,

$$\rho_{m\sigma q\sigma'} = \begin{bmatrix} l & 1 & c \\ -m & q & -q+m \end{bmatrix}^2 \delta_{\sigma\sigma'} \, . \tag{3}$$

Using a recoupling, this can be written in a way that allows one to separate the operators measured using different light and spin polarizations:

$$\rho_{q\sigma'} = \sum_{m\sigma}\langle n_{m\sigma}\rangle\{\tfrac{1}{3}A_0 + \tfrac{1}{2}A_1 qm$$

$$+ \tfrac{1}{2}A_2(q^2-\tfrac{2}{3})[m^2-\tfrac{1}{3}l(l+1)]\}(\tfrac{1}{2}+2\sigma\sigma') \, . \tag{4}$$

Inspection of Eq. (4) shows that its terms have orthogonal dependencies on q and σ' and therefore we can, just as in paper I, define six fundamental linear combinations ρ^{xy} of the primitive integrated intensities $\rho_{q\sigma'}$ that select out terms with simple dependency on m and σ:

$$\rho^{00} \equiv \rho_{1\uparrow} + \rho_{0\uparrow} + \rho_{-1\uparrow} + \rho_{1\downarrow} + \rho_{0\downarrow} + \rho_{-1\downarrow} \, , \tag{5}$$

$$\rho^{01} \equiv \rho_{1\uparrow} + \rho_{0\uparrow} + \rho_{-1\uparrow} - \rho_{1\downarrow} - \rho_{0\downarrow} - \rho_{-1\downarrow} \, , \tag{6}$$

$$\rho^{10} \equiv \rho_{1\uparrow} - \rho_{-1\uparrow} + \rho_{1\downarrow} - \rho_{-1\downarrow} \, , \tag{7}$$

$$\rho^{11} \equiv \rho_{1\uparrow} - \rho_{-1\uparrow} - \rho_{1\downarrow} + \rho_{-1\downarrow} \, , \tag{8}$$

$$\rho^{20} \equiv \rho_{i\uparrow} - 2\rho_{0\uparrow} + \rho_{-1\uparrow} + \rho_{1\downarrow} - 2\rho_{0\downarrow} + \rho_{-1\downarrow} \, , \tag{9}$$

$$\rho^{21} \equiv \rho_{1\uparrow} - 2\rho_{0\uparrow} + \rho_{-1\uparrow} - \rho_{1\downarrow} + 2\rho_{0\downarrow} - \rho_{-1\downarrow} \, , \tag{10}$$

where $\uparrow$ and $\downarrow$ means $\sigma' = \pm\tfrac{1}{2}$. Thus, $x = 0$, 1, and 2 denotes the isotropic spectrum and the circular and linear dichroism, respectively, and $y = 0$ and 1 denotes without and with spin polarization, respectively.

B. Photoemission spectra in LS coupling

It is illustrative to give, in addition to the integrated intensities, the derivation of the complete linear and circular dichroism and the spin polarization in pure LS coupling for a single configuration. In the ground state we assume that the Hund's-rule ground LS term is not mixed with other terms. The results will be given in a form that remains valid when small spin-orbit, crystal-field, and exchange interactions split the ground-state LS term. These results apply directly to the rare earths if the spin-orbit splitting of the final-state terms is smaller than the Coulomb splitting between the terms. The case of observable spin-orbit splitting is treated in Sec. II D.

Take $\langle\psi| = \langle l^n LSM_L M_S|$ and $\langle\psi'| = \langle l^{n-1}\underline{LSM_L M_S}|$ in Eq. (1), then we have, using the graphical representation of the 3-j symbols,[52-54]

$$\langle\psi|l^\dagger_{m\sigma}|\psi'\rangle = \langle LS\|l^\dagger\|\underline{LS}\rangle \quad \text{[graphical symbol]} \quad , \tag{11}$$

where the reduced matrix element of the creation operator is connected to the fractional parentage coefficient:[51]

$$\langle LS\|l^\dagger\|\underline{LS}\rangle$$

$$= (-1)^n[n(2S+1)(2L+1)]^{1/2}(LS\{|\underline{LS}) \, . \tag{12}$$

After substitution of Eq. (11) into (1) and summation of the squared matrix element over $\underline{M}_L$ and $\underline{M}_S$ we obtain, apart from the radial dipole matrix element,

$$I_{q\sigma'}(\underline{LS}) = |\langle LS\|l^\dagger\|\underline{LS}\rangle|^2 \quad \text{[graphical symbols]}$$

$$= |\langle LS\|l^\dagger\|\underline{LS}\rangle|^2 \left\{\sum_x [x] \quad \text{[graphical symbols]} \right\} \left\{\sum_y [y] \quad \text{[graphical symbols]} \right\} \, , \tag{13}$$

$$I_{q\sigma'}(\underline{LS}) = |\langle LS\|l^{\dagger}\|\underline{LS}\rangle|^2 \{\tfrac{1}{3}A_0 a_0(L) + \tfrac{1}{2}A_1 a_1(l\underline{LL})M_L q + \tfrac{1}{6}A_2 a_2(l\underline{LL})(q^2 - \tfrac{2}{3})[M_L^2 - \tfrac{1}{3}L(L+1)]\}$$

$$\times \{\tfrac{1}{2}a_0(S) + 2a_1(\tfrac{1}{2}\underline{SS})M_S\sigma'\} , \tag{14}$$

where

$$a_0(L) = \frac{1}{2L+1} , \tag{15}$$

$$a_1(l\underline{LL}) = \frac{L(L+1)+l(l+1)-\underline{L}(\underline{L}+1)}{2L(L+1)(2L+1)} , \tag{16}$$

$$a_2(l\underline{LL}) = \frac{6[3K(K-1)-4l(l+1)L(L+1)]}{(2L-1)(2L)(2L+1)(2L+2)(2L+3)} , \tag{17}$$

$$K = L(L+1)+l(l+1)-\underline{L}(\underline{L}+1) , \tag{18}$$

and

$$A_0 = a_0(l) , \tag{19}$$

$$A_1 = a_1(1cl) , \tag{20}$$

$$A_2 = a_2(1cl) . \tag{21}$$

The values of A are given in Table I for various transitions.

We can again define six fundamental spectra I^{xy} which are linear combinations of the primitive spectra $I_{q\sigma'}$ that select our terms with simple dependency on M_L and M_S and associated dependency on $\underline{L}$ and $\underline{S}$:

$$I^{00} \equiv I_{1\uparrow} + I_{0\uparrow} + I_{-1\uparrow} + I_{1\downarrow} + I_{0\downarrow} + I_{-1\downarrow} , \tag{22}$$

$$I^{01} \equiv I_{1\uparrow} + I_{0\uparrow} + I_{-1\uparrow} - I_{1\downarrow} - I_{0\downarrow} - I_{-1\downarrow} , \tag{23}$$

$$I^{10} \equiv I_{1\uparrow} - I_{-1\uparrow} + I_{1\downarrow} - I_{-1\downarrow} , \tag{24}$$

$$I^{11} \equiv I_{1\uparrow} - I_{-1\uparrow} - I_{1\downarrow} + I_{-1\downarrow} , \tag{25}$$

$$I^{20} \equiv I_{1\uparrow} - 2I_{0\uparrow} + I_{-1\uparrow} + I_{1\downarrow} - 2I_{0\downarrow} + I_{-1\downarrow} , \tag{26}$$

$$I^{21} \equiv I_{1\uparrow} - 2I_{0\uparrow} + I_{-1\uparrow} - I_{1\downarrow} + 2I_{0\downarrow} - I_{-1\downarrow} . \tag{27}$$

C. Fundamental spectra

In this section we explain that the integrals of the fundamental spectra give the expectation values of the ground-state moments, and that the intensity to a final state measures the alignment in that final state of the ground-state moment with the moment of the core hole created.

We define l_z, $s_{z'}$, and $q_{zz} = l_z^2 - \tfrac{1}{3}l(l+1)$ as one-electron

operators acting only on l-shell functions. L_z, S_z, and Q_{zz} are sums of these over all electrons, and measure only properties of l-shell electrons. When the ground state $\langle \psi|$ is a linear combination of sublevels of an LS term with different M_L and M_S then in Eq. (14) the cross terms are zero, just like they are for L_z and L_z^2. Therefore, we can replace M with $\langle L_z\rangle$ and M^2 with $\langle L_z^2\rangle$ to make the result valid for any state within the LS term.

1. Isotropic spectrum, I^{00}

The spectrum is obtained with unpolarized light ($x = 0$) and without spin detection ($y = 0$). Substitution of Eq. (4) into Eq. (5) gives, for the integrated intensity,

$$\rho^{00} = A_0 \sum_{m\sigma} \langle n_{m\sigma}\rangle = A_0\langle n\rangle , \tag{28}$$

which is proportional to the number of electrons n in the l shell, i.e., the monopole moment. Note that the isotropic spectrum [Eq. (5)] is defined as the sum over all polarizations and not as the average. Because normally we cannot perform absolute intensity measurements, we can only obtain properties per electron, by dividing the polarized signals discussed below by the isotropic signal.

The intensities for $\underline{LS}$ peaks in the isotropic spectrum is obtained by substitution of Eq. (14) into (22):

$$I^{00}(\underline{LS}) = \tfrac{1}{6}A_0 a_0(L)a_0(S)|\langle LS\|l^{\dagger}\|\underline{LS}\rangle|^2 , \tag{29}$$

which measures the parentage of the ground state to the final states.

2. Spin spectrum, I^{01}

In this spectrum the electrical vector q is isotropic ($x = 0$) and it cannot sense the polarization of the valence orbitals. Substitution of Eq. (4) into (6) gives the integrated spin spectrum, which measures the expectation value of the spin magnetic moment:

$$\rho^{01} = 2A_0 \sum_{m\sigma} \langle n_{m\sigma}\rangle\sigma = 2A_0\langle S_{z'}\rangle . \tag{30}$$

The intensities for $\underline{LS}$ peaks are obtained by substitution of Eq. (14) into Eqs. (22) and (23):

$$\frac{I^{01}(\underline{LS})}{I^{00}\underline{LS}} = \frac{a_1(\tfrac{1}{2}\underline{SS})}{a_0(S)}\langle S_{z'}\rangle . \tag{31}$$

The coefficient $a_1(\tfrac{1}{2}\underline{SS})$ gives the alignment of S with the spin $\tfrac{1}{2}$ moment of the hole when they combine to give $\underline{S}$. A negative a_1 means that $\underline{S}$ is large and that S and $\tfrac{1}{2}$ are parallel. For positive a_1 they are antiparallel. So in I^{01}, peaks for final states of high and low spin have opposite signs. The whole spectrum is proportional to $\langle S_{z'}\rangle$.

TABLE I. The values of A_x defined in Eqs. (19)–(21) for the transitions $l \rightarrow c$ in photoemission, where l is the valence shell and c is the continuum shell in XPS (or the core shell in XAS).

	$p \rightarrow s$	$p \rightarrow d$	$d \rightarrow p$	$d \rightarrow f$	$f \rightarrow d$	$f \rightarrow g$
A_0	$\tfrac{1}{3}$	$\tfrac{1}{3}$	$\tfrac{1}{5}$	$\tfrac{1}{5}$	$\tfrac{1}{7}$	$\tfrac{1}{7}$
A_1	$\tfrac{1}{3}$	$-\tfrac{1}{6}$	$\tfrac{1}{10}$	$-\tfrac{1}{15}$	$\tfrac{1}{21}$	$-\tfrac{1}{28}$
A_2	1	$\tfrac{1}{10}$	$\tfrac{1}{10}$	$\tfrac{1}{35}$	$\tfrac{1}{35}$	$\tfrac{1}{84}$

3. Magnetic circular dichroism, I^{10}

In this spectrum no spin polarization is detected ($y = 0$), but the difference in photoemission for right- and left-circular polarization is measured ($x = 1$). The integrated circular dichroism ρ^{10} is obtained by substituting Eq. (4) into (7):

$$\rho^{10} = A_1 \sum_{m\sigma} \langle n_{m\sigma} \rangle m = A_1 \langle L_z \rangle \ , \tag{32}$$

which measures the expectation value of the orbital magnetic moment, just as in x-ray absorption,[10] which is a particle-hole analogue of valence XPS replacing the continuum shell by a core level.

The intensities for $\underline{LS}$ peaks is obtained by substitution of Eq. (14) into Eqs. (22) and (24):

$$\frac{I^{10}(\underline{LS})}{I^{00}(\underline{LS})} = \frac{A_1 a_1 (l \underline{LL})}{A_0 a_0 (L)} M_L$$

$$= \frac{A_1}{A_0} \frac{L(L+1) + l(l+1) - \underline{L}(\underline{L}+1)}{2L(L+1)} \langle L_z \rangle \ . \tag{33}$$

In LS coupling the spectrum is proportional to $\langle L_z \rangle$ and measures the $\underline{L}$ value of the final states.

4. Spin-orbit spectrum, I^{11}

This spectrum, which is sometimes called the optical spin orientation, is measured using both circular polarization ($x = 1$) and spin detection ($y = 1$). The integrated intensity is obtained by substituting Eq. (4) into (8):

$$\rho^{11} = 2A_1 \sum_{m\sigma} \langle n_{m\sigma} \rangle m\sigma = 2A_1 \langle \sum_i l_z(i) s_{z'}(i) \rangle \ . \tag{34}$$

It measures the correlation of the z component of l and the z' component of s. For this effect magnetic polarization is not required. For example, for isotropic ions and $z = z'$ it is simply one-third of the spin-orbit coupling.

The intensities for $\underline{LS}$ peaks is obtained by substitution of Eq. (14) into Eqs. (22) and (25):

$$\frac{I^{11}(\underline{LS})}{I^{00}(\underline{LS})} = \frac{A_1 a_1 (l\underline{LL}) a_1 (\frac{1}{2}\underline{SS})}{A_0 a_0 (L) a_0 (S)} \langle L_z S_{z'} \rangle \ . \tag{35}$$

In the ground state L_z and $S_{z'}$ have to be correlated, which is possible by having $\langle L_z \rangle$ and $\langle S_{z'} \rangle$ both nonzero but when this is not the case spin-orbit coupling can still make $\langle L_z S_{z'} \rangle$ nonzero.

5. Anisotropic spectrum, I^{20}

The anisotropic spectrum or (possibly magnetic) linear dichroism measures the difference in photoemission using perpendicular and parallel linearly polarized light ($x = 2$). The spin is not detected ($y = 0$). This spectrum is present in both ferromagnets and antiferromagnets but also in low-symmetry crystal fields. The integrated linear dichroism ρ^{20} is obtained by substituting Eq. (4) into (9):

$$\rho^{20} = A_2 \sum_{m\sigma} \langle n_{m\sigma} \rangle [m^2 - \tfrac{1}{3} l(l+1)] = A_2 \langle Q_{zz} \rangle \ , \tag{36}$$

where

$$Q_{zz} = \sum_i l_z^2(i) - \tfrac{1}{3} l(l+1) \ , \tag{37}$$

which is (proportional to) the quadrupole moment.

The intensities for $\underline{LS}$ peaks is obtained by substitution of Eq. (14) into Eqs. (22) and (26):

$$\frac{I^{20}(\underline{LS})}{I^{00}(\underline{LS})} = \frac{\frac{1}{3} A_2 a_2 (l\underline{LL})}{A_0 a_0 (L)} [M_z^2 - \tfrac{1}{3} L(L+1)]$$

$$= \frac{A_2}{A_0} \frac{2[3K(K-1) - 8l(l+1)]}{(2L-1)(2L)(2L+2)(2L+3)}$$

$$\times \langle L_z^2 - \tfrac{1}{3} L(L+1) \rangle \ , \tag{38}$$

where K was given in Eq. (18).

6. Anisotropic spin spectrum, I^{21}

In this spectrum we measure spin polarization ($y = 1$) using linearly polarized light ($x = 2$). The integrated intensity is obtained by substituting Eq. (4) into (10):

$$\rho^{21} = 2A_2 \sum_{m\sigma} \langle n_{m\sigma} \rangle [m^2 - \tfrac{1}{3} l(l+1)]\sigma$$

$$= 2A_2 \langle \sum_i q_{zz}(i) s_{z'}(i) \rangle \ . \tag{39}$$

Like ρ^{11}, it has a value if both $S_{z'}$ and Q_{zz} are nonisotropic, but when S is unpolarized there is still a contribution if spin-orbit coupling gives the spin a different value when the electron is along the Z axis or in the XY plane.

The intensities for $\underline{LS}$ peaks is obtained by substitution of Eq. (14) into Eqs. (22) and (27):

$$\frac{I^{21}(\underline{LS})}{I^{00}(\underline{LS})} = \frac{\frac{1}{3} A_2 a_2 (l\underline{LL}) a_1 (\frac{1}{2}\underline{SS})}{A_0 a_0 (L) a_0 (S)}$$

$$\times \langle [L_z^2 - \tfrac{1}{3} L(L+1)] S_{z'} \rangle \ . \tag{40}$$
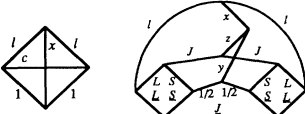
D. Symmetry breaking

In LS coupling one of the great advantages of the analysis in terms of fundamental spectra is that the shape of these spectra is independent of small crystal and exchange fields and temperature effects. So, e.g., the spectrum I^{10} has the same shape [i.e., the $\underline{L}$ dependence in Eq. (33)] in any crystal or exchange field. Only the total intensity changes proportional to $\langle L_z \rangle$ as it should in order to obey the sum rule, Eq. (32). So once the shape of a fundamental spectrum is known (e.g., by our calculations or by experiments) we only have to measure part of the spectrum in order to know the accompanying moment. Note that the shape of, e.g., I^{11} remains the same even when the directions of the light polarization and spin-polarization detection are varied independently. Another symmetry is that $I^{xy}(:)I^{x0}*I^{0y}/I^{00}$. These properties are a consequence of the high symmetry of the problem. When the symmetry is broken the number of fundamental spectra increases and the analysis becomes more complex.

The most important source of breaking of LS symme-

try in $4f$ systems is spin-orbit coupling. In the late rare earths the spin-orbit coupling is so large that different $\underline{LS}$ terms overlap and the spectrum differs considerably from the pure LS coupling case. In that case those spectra I^{xy} that have x and y both different from zero (i.e., I^{11} and I^{21}) are no longer invariant but change depending on the crystal and exchange field. The origin of this can be shown by a derivation of the intensities in LSJ coupling. For Eq. (11) we obtain

$$\langle LSJM|l_{m\sigma}^{\dagger}|\underline{LSJM}\rangle = \langle LS\|l^{\dagger}\|\underline{LS}\rangle \quad \text{(41)}$$

Substitution into Eq. (1) and summation over $\underline{M}$ then gives

$$I_{q\sigma'}=|\langle LS\|l^{\dagger}\|\underline{LS}\rangle|^{2}\sum_{xyz}[xyz] \quad \text{(42)}$$

In the same way as in paper I, we see that $I^{xy}=\sum_{z}I^{xyz}$, where the sum over z is from $|x-y|$ to $(x+y)$ with $x+y+z$ even. This means that $I^{11}=I^{110}+I^{112}$ and $I^{21}=I^{211}+I^{213}$ so these spectra become a sum of two fundamental spectra which have a shape ($\underline{L}$, $\underline{S}$, and $\underline{J}$ dependence) independent of the crystal and exchange field and an intensity proportional to $\langle J_{0}^{(z)}\rangle$, which is the Z component of the monopole, dipole, quadrupole, and octupole moment for $z=0$, 1, 2, and 3, respectively. The monopole moment is a constant but the other moments depend on the fields.

For simplicity we have not plotted I^{110}, I^{112}, I^{211}, and I^{213} separately but they can be calculated and so the experimental I^{11} and I^{21} spectra may be decomposed to determine the associated multipole moments.

Considering the effects of small crystal fields in the LS or LSJ coupling limit it may be surprising that there is, e.g., only one circular dichroism I^{10} whereas there should be three when the symmetry of the fields is low enough. The solution is that there are indeed three different I^{10} spectra (e.g., in the X, Y, and Z directions) but when the crystal field is small the shape of these spectra is the same within the experimental resolution and only their intensity is different. When the crystal field is large enough to mix different J levels in the ground state or to give observable splittings in the final state the shape of the three spectra becomes different. Mathematically we obtain these effects when in the case of small splittings we sum over the final-state $\underline{M}$ values, whereas each $\underline{M}$ state (or rather each point group representation) has its individual intensity when the splittings are observable. This is the same kind of mechanism that increased the number of fundamental spectra going from LS to LSJ coupling when spin-orbit splitting becomes observable. When the crystal-field splitting becomes observable the situation grows more and more complicated, but the sum rules still hold because they hold for all f electron states with either integer or fractional occupation.

E. Angular dependence

The integrals of the six spectra provide six independent moments of the distribution of the occupation numbers $\langle n_{m\sigma}\rangle$. If we could do absolute measurements of the ρ this would be sufficient to determine all $\langle n_{m\sigma}\rangle$ for a p shell. For a d or an f shell more information is needed to determine all occupations. It is instructive to see that this can be obtained from the angular dependence of the photoemission. In Eq. (2), we took the angle-integrated signal by summing over m'. For the angle-resolved signal we omit this summation:

$$\rho_{qm'\sigma'}=\sum_{m\sigma}\langle n_{m\sigma}\rangle\rho_{m\sigma qm'\sigma'}, \quad \text{(43)}$$

where $\rho_{qm'\sigma'}$ is the probability of producing a $cm'\sigma'$ continuum electron. $\rho_{m'\sigma'}$ are the coefficients when we expand the angle dependence of the integrated spectrum in squares of spherical harmonics $|Y_{cm}|^{2}$. (This analysis in cylindrical symmetry implies effectively an integration over φ. More appropriate information can be obtained using the φ dependence when there is, e.g., a crystal field.) Knowing the coefficients $\rho_{m\sigma qm'\sigma'}$ we can determine all $n_{m\sigma}$ by solving Eq. (43). Because only the square of the wave function can be measured we determine effectively $\rho_{qm'\sigma'}+\rho_{q-m'\sigma'}$, which means that $n_{m\sigma}$ and $n_{-m\sigma}$ cannot be separated by isotropic light only. By measuring the dichroism, however, they can be separated, and by measuring the spin of the photoelectron we can separate $n_{m\uparrow}$ from $n_{m\downarrow}$.

Thus, a complete measurement allows one to determine all $\langle n_{m\sigma}\rangle$ with respect to the chosen quantization axis. Integration over the angle or the spin or light polarization gives only "statistical" information, such as $\langle L_{z}\rangle$ or $\langle S_{z}\rangle$. A more complete analysis of the angle dependence of the fundamental spectra is a subject of research for the near future.

III. SPIN-PHOTON POLARIZED $4f$ PHOTOEMISSION

A. Calculational details

In order to illustrate the theory given above we have calculated the spin-photon polarized photoemission from the localized $4f$ levels in rare-earth ions with spherical symmetry in a magnetic field. The results of these calculations, which are presented in Fig. 1, are given for emission to the d continuum ($\Delta l=-1$). The fundamental spectra for emission to the g continuum ($\Delta l=+1$) can be obtained by multiplying those for d emission by a factor 1, $-\frac{3}{4}$, and $\frac{5}{12}$ for $x=0$, 1, and 2, respectively (cf. Table I). Thus, for the fundamental spectra the dependence on c is only a scaling factor.

The photoemission process is given by a transition from the ground state of a configuration f^{n} to a final state with a configuration f^{n-1} plus an electron in the continuum level c. The initial- and final-state configurations are split by the Coulomb interactions $F^{2,4,6}(ff)$ and by spin-orbit interaction $\zeta(f)$,[55-56] but all interactions which involve the shell c are zero. The
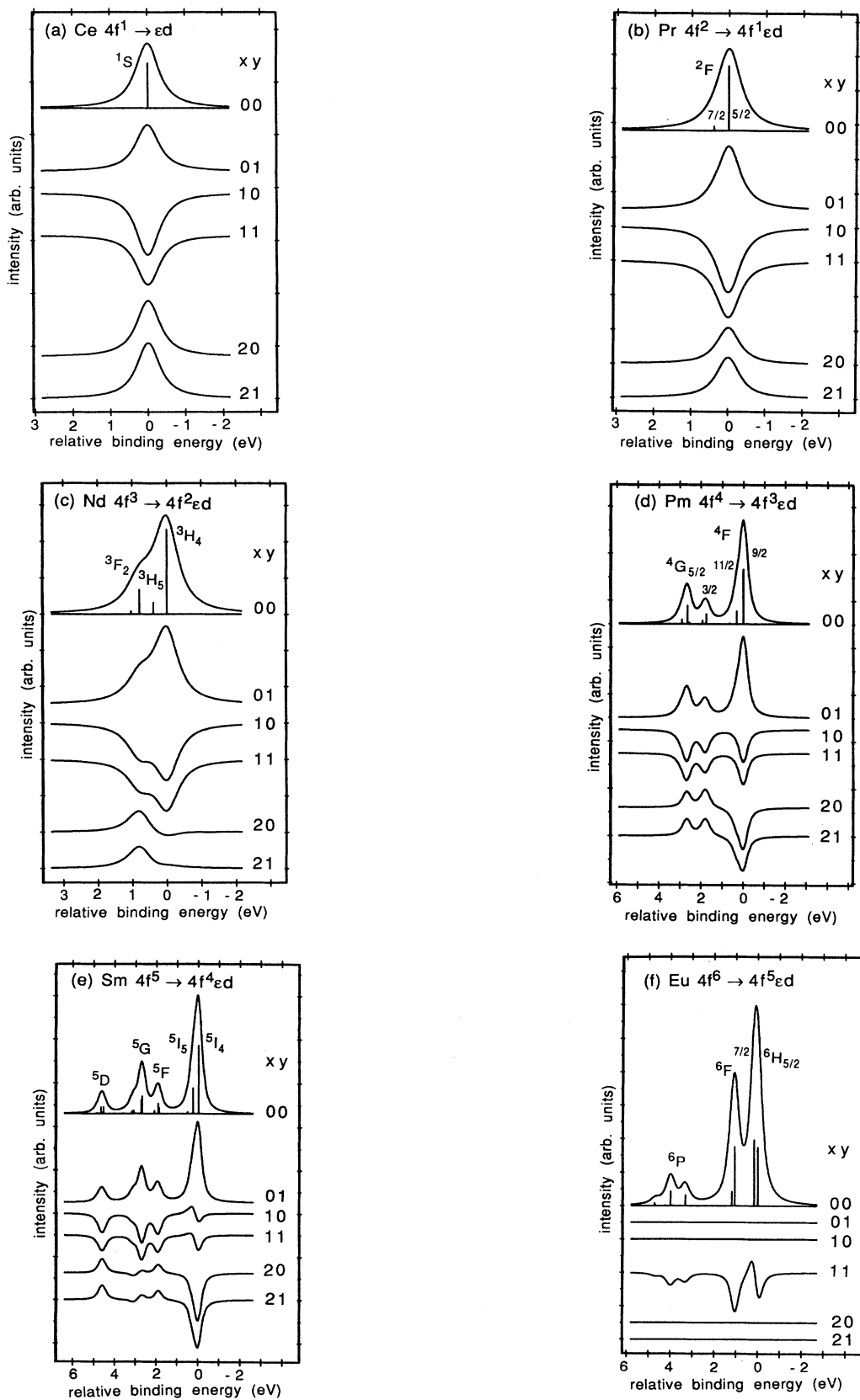
FIG. 1. The fundamental spectra I^{xy} for the $4f \rightarrow \varepsilon d$ photoemission of the rare earths, calculated using Cowan's code (Ref. 59) with the Slater integrals and spin-orbit parameters given in Table II.
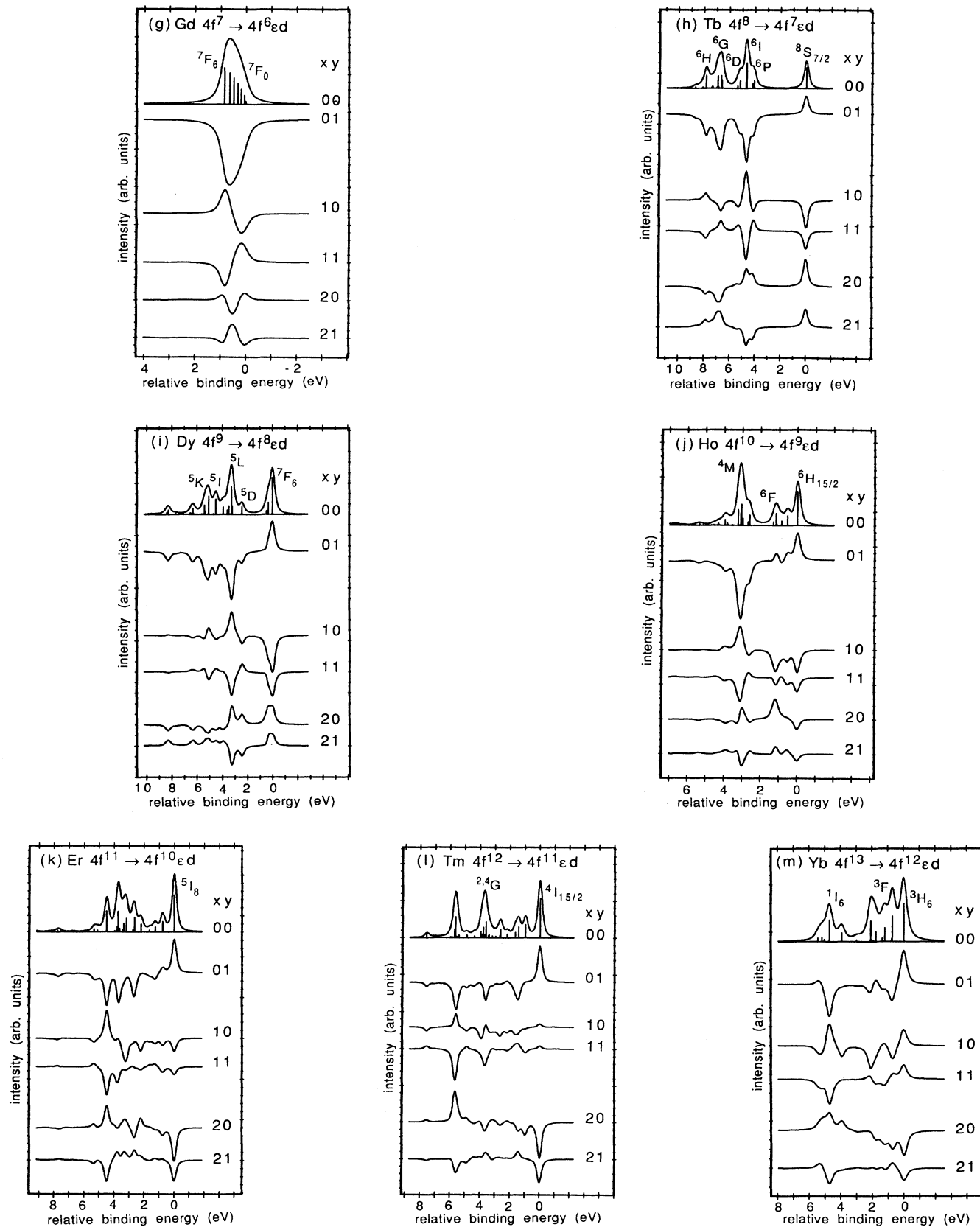
FIG. 1. *(Continued).*

TABLE II. The Hartree-Fock values (eV) of the Slater and spin-orbit parameters for the initial and final states in the $4f$ photoemission of the trivalent rare-earth ions, obtained by Cowan's code (Ref. 59). Γ(XPS) is the experimental value for the Lorentzian broadening of the linewidth (eV) (Ref. 61).

R^{3+}	n	$4f^n$				$4f^{n-1}$				Γ(XPS)
		F^2	F^4	F^6	$\zeta(f)$	F^2	F^4	F^6	$\zeta(f)$	
Ce	1				0.087					0.35
Pr	2	12.228	7.670	5.443	0.102				0.114	0.35
Nd	3	12.726	7.985	5.688	0.119	13.749	8.678	6.221	0.131	0.37
Pm	4	13.199	8.281	5.898	0.136	14.184	8.951	6.427	0.149	0.20
Sm	5	13.650	8.566	6.147	0.155	14.606	9.216	6.609	0.169	0.16
Eu	6	14.085	8.391	6.309	0.175	15.017	9.472	6.781	0.190	0.20
Gd	7	14.507	9.103	6.508	0.197	15.418	9.723	6.966	0.212	0.18
Tb	8	14.917	9.360	6.708	0.221	15.809	9.966	7.082	0.237	0.17
Dy	9	15.318	9.611	6.804	0.246	16.195	10.207	7.270	0.263	0.17
Ho	10	15.709	9.855	6.997	0.273	16.574	10.443	7.449	0.291	0.12
Er	11	16.094	10.094	7.182	0.302	16.946	10.674	7.622	0.320	0.12
Tm	12	16.471	10.330	7.360	0.333	17.314	10.903	7.795	0.352	0.12
Yb	13				0.366	17.679	11.128	7.934	0.386	0.20

atomic values for the Slater and spin-orbit parameters are given in Table II. Transitions with $q=-1$ ($\Delta M=+1$) are excited with right-circularly polarized light (R), and $q=+1$ ($\Delta M=-1$) with left-circularly polarized light (L).[57] The $q=0$ ($\Delta M=0$) transitions are excited by radiation that is linearly polarized along the z axis. According to Eqs. (22)–(27) the isotropic spectrum ($x=0$) is defined as $L+R+Z$, the circular dichroism ($x=1$) as $L-R$, and the linear dichroism ($x=2$) as $L+R-2Z$.

The transition probability for photoemission from a ground state with $M=-J$ and other approximate properties given in Table III have been calculated in intermediate coupling using the programs of Cowan[58,59] with the Slater integrals scaled to 80% of the atomic values to account for intra-atomic relaxation effects.[60] The calculated spectra were convoluted using a Lorentzian width Γ as given in Table II for XPS and 0.8 eV for BIS and a Gaussian of $\sigma=0.085$ eV.[61] The results for the isotropic spectra agree well with earlier calculations[61-65] as well as with experimental results.[61]

TABLE III. The spin and orbital momentum and the z components of the total angular momentum, spin, and orbital magnetic moment and the quadrupole moment for the Hund's-rule ground state f^n ($LSJM$) of the rare earths in pure LSJ coupling.

R^{3+}	n	S	L	$J_z(=-J)$	S_z	L_z	Q_{zz}
Ce	1	0.5	3	−2.5	0.3576	−2.857	4.285
Pr	2	1	5	−4	0.8	−4.8	4.411
Nd	3	1.5	6	−4.5	1.2276	−5.727	1.736
Pm	4	2	6	−4	1.6	−5.6	−1.620
Sm	5	2.5	5	−2.5	1.786	−4.286	−3.095
Eu	6	3	3	−0	0	0	0
Gd	7	3.5	0	−3.5	−3.5	0	0
Tb	8	3	3	−6	−3	−3	5
Dy	9	2.5	5	−7.5	−2.5	−5	5
Ho	10	2	6	−8	−2	−6	2
Er	11	1.5	6	−7.5	−1.5	−6	−2
Tm	12	1	5	−6	−1	−5	−5
Yb	13	0.5	3	−3.5	−0.5	−3	−5

B. Integrated intensities

The integrated intensities of the fundamental spectra are given in Table IV. By using Eqs. (28) and (30), we can obtain $\langle S_z \rangle$ and $\langle L_z \rangle$ from ρ^{01} and ρ^{10}, respectively. Their values are not exactly equal to the values given by the Landé formulas because of the spin-orbit coupling in the ground state. The values for a pure LSJ ground state,

$$\langle L_z \rangle = \langle J_z \rangle \frac{a_1(LSJ)}{a_0(J)}$$

$$= \langle J_z \rangle \frac{J(J+1)+L(L+1)-S(S+1)}{2J(J+1)} , \quad (44)$$

$$\langle S_z \rangle = \langle J_z \rangle \frac{a_1(SLJ)}{a_0(J)}$$

$$= \langle J_z \rangle \frac{J(J+1)+S(S+1)-L(L+1)}{2J(J+1)} , \quad (45)$$

are given in Table III for $\langle J_z \rangle = -J$. Whether $\langle J_z \rangle = -J$ or $+J$ is the actual ground state depends on how J is directed by exchange interaction and the external field. For a ground state $\langle J_z \rangle = J$ the spectra I^{xy} with $x+y$ odd change sign.

Table III shows that L_z is always negative and S_z is positive (negative) for a less (more) than half-filled shell. This is a consequence of the coupling between L and S as given by the third Hund's rule, which has to result in a value $J_z=-J$ for our choice of the magnetic ground state. For $n \leq 5$, L is larger than S, and the antiparallel coupling of L and S results in a negative value for L_z and a positive value for S_z. Therefore, the occupied one-electron states have mainly spin-up and negative l_z. Eu^{3+} f^6 has $J_z=0$ and the only polarized spectrum which is nonzero is I^{11}. Gd^{3+} f^7 has $L_z=0$ and $S_z=-\frac{7}{2}$, and all one-electron states with spin down are occupied. For $n \geq 8$ the parallel coupling of L and S makes L_z and S_z both negative. Thus, the vacant one-electron states have mainly spin-up and positive l_z.

The integrated intensity of the spin-orbit spectrum, ρ^{11},

SPIN POLARIZATION AND MAGNETIC DICHROISM IN. . . . II. . . .

TABLE IV. Integrated intensities ρ^{xy} of the fundamental spectra in Figs. 1 and 2 for the $4f \rightarrow \varepsilon d$ (inverse) photoemission.

	R		Configuration	ρ^{00}	ρ^{01}	ρ^{10}	ρ^{11}	ρ^{20}	ρ^{21}
XPS	Ce	f^1	$^2F_{5/2}$	0.142 86	0.102 04	−0.136 05	−0.108 84	0.122 45	0.122 45
	Pr	f^2	$^3H_4$	0.285 72	0.219 96	−0.227 14	−0.195 55	0.122 05	0.138 47
	Nd	f^3	$^4I_{9/2}$	0.428 57	0.342 15	−0.271 31	−0.241 85	0.047 00	0.069 36
	Pm	f^4	$^5I_4$	0.571 43	0.449 72	−0.265 44	−0.239 84	−0.047 46	−0.025 37
	Sm	f^5	$^6H_{5/2}$	0.714 28	0.499 18	−0.202 24	−0.196 73	−0.089 05	−0.082 96
	Eu	f^6	$^7F_0$	0.857 16	0.000 00	0.000 00	−0.141 51	0.000 00	0.000 00
	Gd	f^7	$^8S_{7/2}$	1.000 00	−0.990 08	−0.001 65	−0.000 60	−0.000 37	−0.002 92
	Tb	f^8	$^7F_6$	1.142 85	−0.840 88	−0.145 57	−0.140 61	0.141 35	0.136 96
	Dy	f^9	$^6H_{15/2}$	1.285 70	−0.690 28	−0.242 09	−0.231 72	0.138 89	0.133 25
	Ho	f^{10}	$^5I_8$	1.428 57	−0.547 30	−0.289 73	−0.275 98	0.051 30	0.048 88
	Er	f^{11}	$^4I_{15/2}$	1.571 43	−0.419 13	−0.287 29	−0.279 88	−0.060 64	−0.057 30
	Tm	f^{12}	$^3H_6$	1.714 29	−0.283 13	−0.238 53	−0.235 94	−0.144 15	−0.141 56
	Yb	f^{13}	$^2F_{7/2}$	1.857 15	−0.142 85	−0.142 86	−0.142 86	−0.142 86	−0.142 85
BIS	Pr	f^2	$^3H_4$	1.714 28	0.219 96	−0.227 13	0.195 55	−0.122 05	0.138 47
	Er	f^{11}	$^4I_{15/2}$	0.428 57	−0.419 12	−0.287 29	0.279 88	0.060 65	−0.057 30

which is proportional to the expectation value of $l \cdot s$, is always negative because the spin-orbit interaction couples l and s antiparallel.

The quadrupole moment can be obtained from the integrated intensity of the linear dichroism, ρ^{20}, by using Eq. (36). For the pure Hund's-rule LSJ ground state we can prove, using the same approach as in Ref. 66, that

$$Q_{zz} = \frac{2(2l+1-n)\pm(2l+1)}{3(2L-1)}$$

$$\times (2J+1)a_2(LSJ)[M^2 - \tfrac{1}{3}J(J+1)] \qquad (46)$$

with the negative (positive) sign for less (more) than half-filled shells. The values of Q_{zz} are given in Table III, and it is clear that they change sign for quarter-filled shells. A positive value of Q_{zz} means that high values of $|m|$ are occupied which makes the ion flat in the XY plane. A negative value corresponds to an elongation along the Z axis. Thus, Q_{zz} is nonzero in ferro- and antiferromagnets as well as in anisotropic crystal fields.

C. Peak intensities

The peak intensities in the multiplet structure of the fundamental spectra give information about the correlation of the momenta LS in the ground state with the moments of the ejected electron (or of the hole left behind) when a transition is made to a final state $\underline{LS}$. The spin spectrum gives the alignment of S with the spin $\frac{1}{2}$ moment of the hole created. From Eq. (31) we see that the final states with low spin ($\underline{S} = S - \frac{1}{2}$) and high spin ($\underline{S} = S + \frac{1}{2}$) have intensities proportional to $S+1$ and $-S$, respectively, times $\langle S_z \rangle I^{00}$. For $n \leq 6$ there are only low-spin final states, therefore the spin spectrum will be proportional to the isotropic spectrum, where all peaks have a positive intensity. This proportionality may make it hard to ensure that the spin spectrum has been measured instead of the isotropic spectrum. For $n \geq 7$, the sign of $\langle S_z \rangle$ is reversed, and the low-spin final states have

negative intensities, whereas the high-spin final states have positive intensities. So, in the spectra from Tb f^8 to Yb f^{13} (Fig. 1) the high-spin Hund's-rule state gives a positive peak at the low binding energy side of the spin spectrum.

The circular dichroism gives the alignment of L with the orbital momentum l of the created hole when they combine to give $\underline{L}$. Thus, the dichroism is determined only by the orbital momenta L and $\underline{L}$ and we see from Eq. (33) that high $\underline{L}$ values give a peak opposite to that of low $\underline{L}$ values. From Eq. (33) we also see that, in theory, in this pure LS coupling case we do not need the integral over the whole spectrum to calculate $\langle L_z \rangle$ but if we know L and $\underline{L}$ the integral over one $\underline{LS}$ peak is sufficient if it is clearly separated from other peaks.

In the spectra from Ce f^1 to Pm f^4 (Fig. 1) all peaks have a negative intensity because $L \geq \underline{L}$ for $n \leq 4$. For f^5 the intensity to ^5I is zero according to Eq. (33), but the transition is split into a positive and a negative peak by spin-orbit coupling.

Even when the integrated signal is small, a fundamental spectrum can have large positive and negative peaks, e.g., in Tb f^8. In Gd f^7, where the integral is zero ($L_z = 0$), the circular dichroism shows a strong dispersivelike structure due to the J dependence (Fig. 1).

Figure 1 shows that the spin-orbit spectra and the circular dichroism spectra have a similar appearance. With small spin-orbit interaction we have $I^{11}(:)I^{10}*I^{01}/I^{00}$, and when there are only low-spin final states ($n \leq 7$) the spin-orbit spectrum is proportional to the circular dichroism. There are larger differences for $n > 7$ because the high- and low-spin states have opposite signs and because the spin-orbit interaction increases along the $4f$ series.

The linear dichroism gives the alignment of the quadrupoles of L and l when they couple to a total $\underline{L}$. The value is positive when L and l are parallel or antiparallel (high and low values of $\underline{L}$) and negative when they are perpendicular (intermediate $\underline{L}$).

If the spin-orbit coupling is small, the anisotropic spin spectrum resembles the linear dichroism in the same way as the circular dichroism resembles the spin-orbit spectrum. Thus, if we would measure the spectra with the aim to determine the symmetries of the final states then, for vanishing spin-orbit splitting, it is only necessary to measure I^{00}, I^{10}, I^{20}, and I^{01}. The spectra I^{11} and I^{21}, both photon and spin polarized, are simply products of these, $I^{x1}(:)I^{x0*}I^{01}/I^{00}$, and contain no new information. However, the absolute (integrated) intensities of these spectra do contain independent information on the ground state.

IV. SPIN-PHOTON POLARIZED INVERSE PHOTOEMISSION

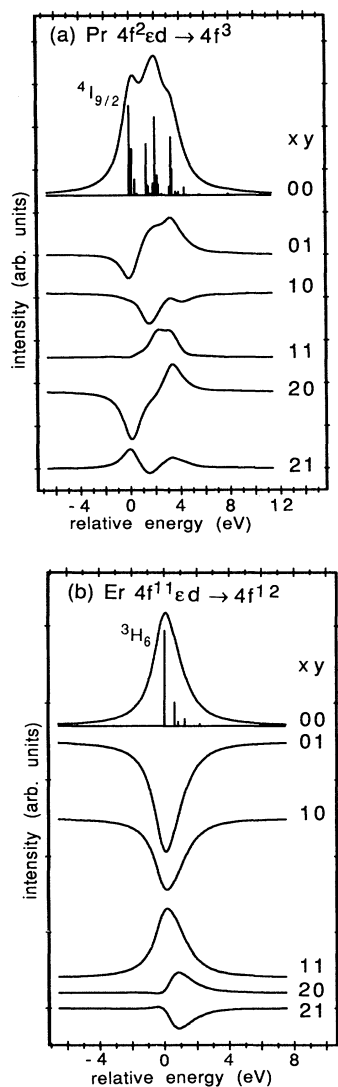In inverse photoemission or bremsstrahlung isochromat spectroscopy (BIS), the sample is irradiated with

FIG. 2. The fundamental spectra I^{xy} for the $\varepsilon d \rightarrow 4f$ inverse photoemission of Pr and Er, calculated using Cowan's code (Ref. 59) with the Slater integrals and spin-orbit parameters given in Table II.

a monochromatic beam of electrons which can decay into the incompletely filled valence band under emission of a photon.[67] The photon helicity can be analyzed using a polarimeter,[68] a Goedkoop filter,[69] an x-ray phase plate,[70] or a multilayer device.[71,72]

The formulas for BIS are obtained in a way analogous to those for XPS but give the properties of the holes instead of the electrons and q and σ' have opposite signs and so ρ^{xy} (and I^{xy}) change sign when $x + y$ is even, except for ρ^{00} (and I^{00}), which is proportional to the number of electrons in XPS and the number of holes in BIS (cf. Table IV). With respect to the number of peaks and the magnitude of the effects, the BIS spectra of f^n are much like the XPS spectra of f^{14-n} because of their particle-hole equivalence. They do, of course, differ in the J value of the Hund's-rule ground state. It is interesting to note that if we know L_z per electron from XPS and L_z per hole for BIS we can obtain L_z and the number of electrons in the ground state, without an absolute intensity measurement.

To calculate the inverse photoemission we included in the initial state an electron in the continuum state c whereas the final-state configuration is f^{n+1}. The results for the fundamental spectra are shown in Fig. 2 for the two examples Pr f^2 and Er f^{11} and the integrated intensities are given in Table IV. The analysis of these BIS spectra is the same as for photoemission, bearing in mind the particle-hole equivalence. For example, in Er f^{11} only low-spin states are possible and $L > \underline{L}$, which results in a completely negative spin spectrum and magnetic circular dichroism, respectively.

V. PROSPECTS

Circular magnetic dichroism in valence-band photoemission has been observed in Fe (Ref. 73) and Co,[74] although these elements are relatively unfavorable. As we have seen, XPS is more suited for less than half-filled shells and BIS for more than half-filled shells. Circular dichroism in $4f$ photoemission has been reported in Gd, where it is in agreement with atomic multiplet calculations.[75] In spin-resolved photoemission much effort has been devoted to Ni and Fe metals, alloys, and overlayers,[76,77] and also to Gd metal, where the (anti)parallel coupling between bulk and surface spins has been studied.[78−82] Thus, so far polarized photoemission experiments have been restricted to specific model compounds due to the low count rate and cumbersomeness of spin detectors and the lack of suitable sources for circularly polarized x rays. However, this situation is changing rapidly. High photon fluxes have become available from insertion devices, such as wigglers and undulators, compact spin detectors have been developed,[83] and a high degree of circular polarization can be obtained by using the off-plane synchrotron radiation from bending magnets or by using helical or asymmetric undulators.[84] Beam lines are now specially optimized for circular polarized soft x rays.[85] It is therefore expected that the importance of both spin polarization and circular dichroism in the study of magnetic properties will increase strongly over the next few years.[86]

TABLE V. The expectation values of the number of d electrons, spin, and orbital magnetic moment for Fe, Co, and Ni metal (Refs. 15 and 94). The integrated intensity predicted for the spin spectrum and the magnetic circular dichroism normalized to the isotropic signal for a $3d \rightarrow \varepsilon d$ transition. For the $3d \rightarrow \varepsilon g$ transition ρ^{10} has to be multiplied by $-\frac{2}{3}$.

	$\langle n \rangle$	$\langle S_z \rangle$	$\langle L_z \rangle$	XPS ρ^{01}/ρ^{00}	ρ^{10}/ρ^{00}	BIS ρ^{01}/ρ^{00}	ρ^{10}/ρ^{00}
Fe	7.3	-2.13	-0.08	-0.584	-0.0055	-1.58	-0.015
Co	8.4	-1.52	-0.14	-0.362	-0.0083	-1.90	-0.044
Ni	9.4	-0.57	-0.053	-0.121	-0.0028	-1.90	-0.044

The $3d$, $4f$, and $5f$ materials form three classes with distinctly different magnetic properties. In the $4f$ compounds, where the crystal-field interaction is small, S and L can be combined to a total J value as given by Hund's rule, and the spin and orbital magnetic moment are both large. In $5f$ compounds the crystal-field and spin-orbit interaction are of comparable magnitude, and mixing of different J levels becomes important.[87] Hybridization is larger than in $4f$ systems, but the valence-band photoemission still shows distinct multiplet structure.[88] In the $3d$ transition metals the spin-orbit interaction is relatively smaller than in $5f$ systems and it is therefore easily quenched by crystal fields and hybridization, which results in a large reduction of orbital magnetic moment. Probably spin-photon polarized spectroscopy is important in all three classes but our present analysis applies most directly to $4f$ systems. For the analysis of $3d$ transition-metal systems one may use either a one-electron band-structure model or an Anderson impurity model,[89,90] which is a localized approach that includes a set of configurations of the type d^{n-1}, d^n, d^{n+1}, etc. The one-electron model reproduces the band structure of the spin-resolved photoemission,[91] but fails to explain the satellite structure in the Ni $2p$ and $3p$ CMXD.[92] The localized approach gives a good agreement in this case,[12,13] and also for the Ni $2p$ and $3p$ CDXPS,[50] and the resonant photoemission decay from the $2p$ level of Ni metal.[93]

The equations for the integrated intensities are independent of the choice of the wave function. Thus, they provide the expectation values of the orbital, spin, and quadrupole moments without a detailed analysis of the spectrum. Conversely, if the expectation values of the angular momenta (per electron/hole) are known, they can be used to predict the integrated intensities of the fundamental spectra. As an example, Table V shows the values of $\langle S_z \rangle$, $\langle L_z \rangle$, and $\langle n \rangle$ for Fe, Co, and Ni metal[15,94] together with the resulting integrated spin spectrum and magnetic circular dichroism. It is clear that the integrated $3d$ spin signal is large and increases from Ni to Fe. The circular dichroism is small because the orbital momentum is quenched. Table V gives also the predicted values for BIS which are much larger than for XPS.

VI. CONCLUSIONS

We have shown that the valence-band photoemission of correlated materials can be fruitfully analyzed in terms of six fundamental spectra. The interpretation of these spectra is relatively simple in the case of a small spin-orbit interaction (LS coupling). Then, the spin spectrum is determined by the alignment of S and $\underline{S}$, and shows high- and low-spin final states with opposite signs. For less than half-filled shells the final states can have only one spin value, and the spin spectrum is proportional to the isotropic spectrum. The circular dichroism is determined by the alignment of L and $\underline{L}$, and the peak intensity increases with $\underline{L}$. The linear dichroism measures the alignment of the quadrupoles. When the spin-orbit interaction is small compared to the Coulomb interactions the shape of the spin-orbit spectrum and the anisotropic spin spectrum are similar to the circular and linear dichroism, respectively, except that high- and low-spin final states have opposite signs, which are given by the spin spectrum. Different relations, but of the same type, were found in deep core-hole photoemission (paper I). There, the spin spectrum resembled the circular dichroism but with opposite signs for the spin-orbit split edges, but the anisotropic spin spectrum was not similar to the linear dichroism.

We have derived general expressions for the integrated intensities of the six fundamental spectra, which relate them to the expectation values of the spin and orbital moments in the ground state. Each fundamental spectrum measures a distinctly different operator. These sum rules provide a powerful tool in the analysis of the photoemission from an open shell because they give the values of physical quantities, independent of theoretical models such as the localized or the delocalized approach. In the core-level spectra the integrated intensities are zero because the expectation values of these operators are zero for a closed shell.

We have illustrated the theory with calculated fundamental spectra of the rare earths, where the multiplet structure of the $4f$ photoemission shows a strong polarization dependence. These fundamental spectra for spherical symmetry at $T=0$ K provide a useful basis for future analysis because the fundamental spectra at finite temperature and in weak crystal field maintain the same shape and only change intensity proportional to the expectation values of the ground-state moments. In $3d$ and $5f$ materials the fundamental spectra lose their property of having a constant shape and then their importance is the fact that their integrals are proportional to the expectation value of simple operators, at least if the $3d$ and $5f$ emission can be separated from the emission from other bands.

We have discussed the particle-hole analogy between XPS and BIS. The former measures L_z and S_z per electron, whereas the latter measures L_z and S_z per hole [just as in x-ray-absorption spectroscopy (XAS)]. The combination of both techniques yields the total values, XPS gives a larger effect for less than half-filled shells, whereas BIS give a larger effect for more than half-filled shells.

Interesting applications may include the determination of the orbital and spin magnetic moment of surface layers because photoemission is more surface sensitive than, e.g., x-ray absorption. The strong circular dichroism signal in rare earths and actinides combined with the recent

availability of intense sources of polarized x rays, such as helical and crossed undulators, make it possible to study samples with a short lifetime, small size, or dilute concentration. The $4f$ or $5f$ partial yield, which can be obtained by collecting all high kinetic-energy electrons above a certain threshold value, can be applied in photo-electron microscopy to measure the spatial resolution of the magnetic domain structure of ferro- and ferrimagnetic materials.

Note added in proof. Very recently the concept of the orbital momentum sum rules has been elegantly applied to resonant x-ray scattering.[95]

[1] L. M. Falicov, D. T. Pierce, S. D. Bader, R. Gronsky, K. B. Hathaway, H. J. Hopster, D. N. Lambeth, S. S. P. Parkin, G. Prinz, M. Salamon, I. K. Schuller, and R. H. Victoria, J. Mater. Res. **5**, 1299 (1990).

[2] J. Jensen and A. R. Mackintosh, *Rare Earth Magnetism, Structures and Excitations* (Oxford University Press, New York, 1991).

[3] G. H. Lander, Phys. Scr. **44**, 33 (1991).

[4] P. M. Platzman and N. Tzoar, Phys. Rev. B **2**, 3356 (1970).

[5] F. deBergevin and M. Brunel, Phys. Lett. **39A**, 141 (1972).

[6] M. Blume, J. Appl. Phys. **57**, 3614 (1985).

[7] M. Blume and D. Gibbs, Phys. Rev. B **37**, 1779 (1988).

[8] D. Gibbs, D. R. Harshmann, E. D. Isaacs, D. B. McWhan, D. Mills, and C. Vettier, Phys. Rev. Lett. **61**, 1241 (1988).

[9] D. B. McWhan, C. Vettier, E. D. Isaacs, G. E. Ice, D. P. Siddons, J. B. Hastings, C. Peters, and O. Vogt, Phys. Rev. B **42**, 6007 (1990).

[10] B. T. Thole, P. Carra, F. Sette, and G. van der Laan, Phys. Rev. Lett. **68**, 1943 (1992); B. T. Thole and G. van der Laan, *ibid.* **70**, 2499 (1993).

[11] C. T. Chen, F. Sette, Y. Ma, and S. Modesti, Phys. Rev. B **42**, 7262 (1990).

[12] T. Jo and G. A. Sawatzky, Phys. Rev. B **43**, 8771 (1991).

[13] G. van der Laan and B. T. Thole, J. Phys.: Condens. Matter **4**, 4181 (1992).

[14] P. J. Brown, J. Phys. I (France) **1**, 1529 (1991).

[15] O. Ericksson, B. Johansson, R. C. Albers, A. M. Boring, and M. S. S. Brooks, Phys. Rev. B **41**, 11 807 (1990); **42**, 2707 (1990).

[16] G. van der Laan and B. T. Thole, Phys. Rev. Lett. **60**, 1977 (1988); B. T. Thole and G. van der Laan, Phys. Rev. B **38**, 3158 (1988); Phys. Rev. A **38**, 1943 (1988).

[17] P. Carra, B. T. Thole, M. Altarelli, and X. Wang, Phys. Rev. Lett. **70**, 694 (1993).

[18] H. Ebert, P. Strange, and B. L. Gyorffy, J. Appl. Phys. **63**, 3055 (1988); Z. Phys. B **73**, 77 (1988).

[19] S. P. Collins, M. J. Cooper, A. Brahmia, D. Laundy, and T. Pitkanen, J. Phys.: Condens. Matter **1**, 323 (1989).

[20] H. Ebert and R. Zeller, Physica B **161**, 191 (1989); Phys. Rev. B **42**, 2744 (1990); H. Ebert, B. Drittler, R. Zeller, and G. Schütz, Solid State Commun. **69**, 485 (1989).

[21] F. Baudelet, E. Dartyge, A. Fontaine, C. Brouder, G. Krill, J. P. Kappler, and M. Piecuch, Phys. Rev. B **43**, 5857 (1991).

[22] C. Brouder and M. Hikam, Phys. Rev. B **43**, 3809 (1991).

[23] C. R. Natoli (private communication).

[24] B. T. Thole, G. van der Laan, and G. A. Sawatzky, Phys. Rev. Lett. **55**, 2086 (1985).

[25] G. van der Laan, B. T. Thole, G. A. Sawatzky, J. B. Goedkoop, J. C. Fuggle, J. M. Esteva, R. C. Karnatak, J. P. Remeika, and H. A. Dabkowska, Phys. Rev. B **34**, 6529 (1986).

[26] G. van der Laan, in *Giant Resonances in Atoms, Molecules and Solids,* Vol. 151 of *NATO Advanced Study Institute Series B: Physics,* edited by J. P. Connerade (Plenum, New York, 1987),

p. 447.

[27] J. B. Goedkoop, J. C. Fuggle, B. T. Thole, G. van der Laan, and G. A. Sawatzky, J. Appl. Phys. **64**, 5595 (1988).

[28] J. B. Goedkoop, B. T. Thole, G. van der Laan, G. A. Sawatzky, F. M. F. de Groot, and J. C. Fuggle, Phys. Rev. B **37**, 2086 (1988).

[29] T. Jo and S. Imada, J. Phys. Soc. Jpn. **58**, 1922 (1989).

[30] G. van der Laan, Phys. Scr. **41**, 574 (1990).

[31] G. van der Laan and B. T. Thole, Phys. Rev. B **42**, 6670 (1990).

[32] G. van der Laan, in *Proceedings of the 2nd European Conference on Progress in X-Ray Synchrotron Radiation Research,* edited by A. Balerna, E. Bernieri, and S. Mobilio (SIF, Bologna, 1990), Vol. 25, p. 243.

[33] S. Imada and T. Jo, J. Phys. Soc. Jpn. **59**, 3358 (1990).

[34] F. Sette, C. T. Chen, Y. Ma, S. Modesti, and N. V. Smith, in *X-ray and Inner-Shell Processes (Knoxville, TN, 1990),* Proceedings of the X-90 Conference, edited by T. A. Carlson, M. A. Krause, and S. T. Manson, AIP Conf. Proc. No. 215 (AIP, New York, 1990), p. 787.

[35] P. Carra and M. Altarelli, Phys. Rev. Lett. **64**, 1286 (1990).

[36] G. van der Laan and B. T. Thole, Phys. Rev. B **43**, 13 401 (1991).

[37] P. Carra, B. N. Harmon, B. T. Thole, M. Altarelli, and G. A. Sawatzky, Phys. Rev. Lett. **66**, 2495 (1991).

[38] M. Sacchi, O. Sakho, and G. Rossi, Phys. Rev. B **43**, 1276 (1991).

[39] T. Jo, Synchrotron Radia. News **5**, 21 (1992).

[40] J. P. Hannon, G. T. Trammel, M. Blume, and Doon Gibbs, Phys. Rev. Lett. **61**, 1245 (1988); C. Kao, J. B. Hastings, E. D. Johnson, D. P. Siddons, G. C. Smith, and G. A. Prinz, *ibid.* **65**, 373 (1990).

[41] J. Bonarski and J. Karp, J. Phys.: Condens. Matter **1**, 9261 (1989).

[42] D. P. Siddons, M. Hart, Y. Amemiya, and J. B. Hastings, Phys. Rev. Lett. **64**, 1967 (1990).

[43] L. Baumgarten, C. M. Schneider, H. Petersen, F. Schäfers, and J. Kirschner, Phys. Rev. Lett. **65**, 492 (1990).

[44] G. van der Laan, J. Phys.: Condens. Matter **3**, 1015 (1991).

[45] G. van der Laan, Phys. Rev. Lett. **66**, 2527 (1991).

[46] B. T. Thole and G. van der Laan, Phys. Rev. B **44**, 12 424 (1991).

[47] B. T. Thole and G. van der Laan, Phys. Rev. Lett. **67**, 3306 (1991).

[48] S. Imada and T. Jo, J. Phys. Soc. Jpn. **60**, 2843 (1991).

[49] H. Ebert, L. Baumgarten, C. M. Schneider, and J. Kirschner, Phys. Rev. B **44**, 4406 (1991).

[50] G. van der Laan, M. A. Hoyland, M. Surman, C. F. J. Flipse, and B. T. Thole, Phys. Rev. Lett. **69**, 3827 (1992).

[51] B. R. Judd, *Second Quantization and Atomic Spectroscopy* (Johns Hopkins Press, Baltimore, 1967).

[52] A. P. Yutsis, I. B. Levinson, and V. V. Vanagas, *Mathematical Apparatus of the Theory of Angular Momentum* (Israel Program for Scientific Translation, Jerusalem, 1962).

[53]D. M. Brink and G. R. Satchler, *Angular Momentum* (Oxford University Press, London, 1962).

[54]I. Lindgren and J. Morrison, *Atomic Many Body Theory*, Vol. 13 of Springer Series in Chemical Physics (Springer, New York, 1982).

[55]See, e.g., B. G. Wybourne, *Spectroscopic Properties of Rare Earths* (Interscience, New York, 1965); G. H. Dieke, *Spectra and Energy Levels of Rare Earth Ions in Crystals* (Wiley, New York, 1968).

[56]B. T. Thole, G. van der Laan, J. C. Fuggle, G. A. Sawatzky, R. C. Karnatak, and J. M. Esteva, Phys. Rev. B **32**, 5107 (1985).

[57]This convention is different than the one we used in Phys. Rev. B **43**, 13 401 (1991).

[58]R. D. Cowan, J. Opt. Soc. Am. **58**, 808 (1968).

[59]R. D. Cowan, *The Theory of Atomic Structure and Spectra* (University of California Press, Berkeley, 1981).

[60]D. W. Lynch and R. D. Cowan, Phys. Rev. B **36**, 9228 (1987).

[61]J. K. Lang, Y. Baer, and P. A. Cox, J. Phys. F **11**, 121 (1981).

[62]E. I. Zabolotskii, Yu. P. Irkhin, and L. D. Finkel'shtein, Fiz. Tverd. Tela (Leningrad) **16**, 1142 (1974) [Sov. Phys. Solid State **16**, 733 (1974)].

[63]M. Campagna, G. K. Wertheim, and Y. Baer, in *Photoemission in Solids II*, edited by L. Ley and M. Cardona (Springer-Verlag, Berlin, 1979).

[64]F. Gerken, J. Phys. F **13**, 703 (1983).

[65]F. Meier and B. P. Zakharchenya, *Optical Orientation* (North-Holland, Amsterdam, 1984).

[66]R. D. Cowan, *The Theory of Atomic Structure and Spectra* (Ref. 59), Sec. 12.8.

[67]P. A. Cox, J. K. Lang, and Y. Baer, J. Phys. F **11**, 113 (1981).

[68]T. Koide, T. Shidara, M. Yuri, N. Kandaka, and H. Fukutani, Appl. Phys. Lett. **58**, 2592 (1991); Rev. Sci. Instrum. **63**, 1458 (1992).

[69]J. B. Goedkoop, J. C. Fuggle, B. T. Thole, G. van der Laan, and G. A. Sawatzky, Nucl. Instrum. Methods Phys. Res. A **273**, 429 (1988).

[70]Boris W. Batterman, Phys. Rev. B **45**, 12 677 (1992).

[71]J. B. Kortright and J. H. Underwood, Nucl. Instrum. Methods Phys. Res. A **291**, 272 (1990).

[72]E. Gluskin, Rev. Sci. Instrum. **63**, 1523 (1992).

[73]C. M. Schneider, M. S. Hammond, P. Schuster, A. Cebollada, R. Miranda, and J. Kirschner, Phys. Rev. B **44**, 12 066 (1991).

[74]J. Bansmann, C. Westphal, M. Getzlaff, F. Fegel, and G. Schönhense, J. Magn. Magn. Mater. **104-107**, 1691 (1992).

[75]K. Starke, E. Navas, L. Baumgarten, and G. Kaindl (unpublished).

[76]R. Feder, *Polarized Electrons in Surface Physics* (World Scientific, Singapore, 1985).

[77]J. Kischner, *Polarized Electrons at Surfaces* (Springer-Verlag, Heidelberg, 1985).

[78]D. Weller, S. F. Alvarado, W. Gudat, K. Schröder, and M. Campagna, Phys. Rev. Lett. **54**, 1555 (1985).

[79]C. Carbone and E. Kisker, Phys. Rev. B **36**, 1280 (1987).

[80]M. Taborelli, R. Allenspach, G. Boffa, and M. Landolt, Phys. Rev. Lett. **56**, 2869 (1986).

[81]D. Weller and S. F. Alvarado, Phys. Rev. B **37**, 9911 (1988).

[82]T. Kachel, R. Rochow, W. Gudat, R. Jungblut, O. Rader, and C. Carbone, Phys. Rev. B **45**, 7267 (1992).

[83]D. T. Pierce, R. J. Celotta, M. H. Kelley, and J. Unguris, Nucl. Instrum. Methods Phys. Res. A **266**, 550 (1988).

[84]M. A. Green, Nucl. Instrum. Methods Phys. Res. A **319**, 83 (1992).

[85]C. T. Chen, Rev. Sci. Instrum. **63**, 1229 (1992).

[86]I. H. Munro, C. A. Boardman, and J. C. Fuggle, *World Compendium of Synchrotron Radiation Facilities* (European Synchrotron Radiation Society, Paris, 1991).

[87]J. H. van Vleck, *Theory of Electric and Magnetic Susceptibilities* (Oxford University Press, Oxford, 1932).

[88]F. Gerken and J. Schmidt-May, J. Phys. F **13**, 1571 (1983).

[89]J. Hubbard, Proc. R. Soc. London Ser. A **276**, 238 (1963); **277**, 237 (1964).

[90]A. Kotani, T. Jo, and J. C. Parlebas, Adv. Phys. **37**, 37 (1988).

[91]C. S. Wang and J. Callaway, Phys. Rev. B **9**, 4897 (1974); **15**, 298 (1977).

[92]N. V. Smith, C. T. Chen, F. Sette, and L. F. Mattheiss, Phys. Rev. B **46**, 1023 (1992).

[93]G. van der Laan, M. Surman, M. A. Hoyland, C. F. J. Flipse, B. T. Thole, Y. Seino, H. Ogasawara, and A. Kotani, Phys. Rev. B **46**, 9336 (1992).

[94]G. Treglia, F. Ducastelle, and D. Spanjaard, J. Phys. (Paris) **43**, 341 (1982).

[95]Jin Luo, G. T. Trammell, and J. P. Hannon (unpublished).